Published in final edited form as:
Biomaterials. 2014 February ; 35(5): . doi:10.1016/j.biomaterials.2013.10.008.

Geometric Control of Vimentin Intermediate Filaments

Shagufta H. Shabbir[#a], **Megan M. Cleland**[#b], **Robert D. Goldman**[b,*], and **Milan Mrksich**[a,b,*]
[a]Departments of Biomedical Engineering and Chemistry, Northwestern University, IL, United States

[b]Department of Cell and Molecular Biology, Northwestern University, IL, United States

[#] These authors contributed equally to this work.

Abstract

Significant efforts have addressed the role of vimentin intermediate filaments (VIF) in cell motility, shape, adhesion and their connections to microfilaments (MF) and microtubules (MT). The present work uses micropatterned substrates to control the shapes of mouse fibroblasts and demonstrates that the cytoskeletal elements are dependent on each other and that unlike MF, VIF are globally controlled. For example, both square and circle-shaped cells have a similar VIF distribution while MF distributions in these two shapes are quite different and depend on the curvature of the shape. Furthermore, in asymmetric and polarized shaped cells VIF avoid the sharp edges where MF are highly localized. Experiments with vimentin-null mouse embryonic fibroblasts (MEFs) adherent to polarized (teardrop) and un-polarized (dumbbell) patterns show that the absence of VIF alters microtubule organization and perturbs cell polarity. The results of this study also demonstrate the utility of patterned substrates for quantitative studies of cytoskeleton organization in adherent cells.

Keywords

Cell Adhesion; Micropatterning; Image Analysis; Mechanical Properties; Cytoskeleton

Introduction

The cytoskeleton is a polymeric scaffold that gives the cell structure, mediates its physical attachment to substrates and regulates signaling pathways. It is composed of actin-containing microfilaments (MF), intermediate filaments (IF) containing one or more proteins and tubulin-containing microtubules (MT). These cytoskeletal elements are connected to each other with “plakin type” linkers [1-3]; yet most studies do not treat the cytoskeleton as a single integrated structure but rather focus on one of the distinct elements. Recent studies have revealed the interdependence of cytoskeletal systems and have motivated efforts to explore their structural and functional relationships [3-5]. For example, it has been shown

[*]Corresponding authors: Department of Cell and Molecular Biology, Northwestern University, Ward Building Room # 11-145, 303 E. Chicago Avenue, Chicago, IL 60611, United States r-goldman@northwestern.edu Phone: 312-503-4215 Fax: 312-503-0954 M. Mrksich Departments of Biomedical Engineering and Chemistry, Northwestern University, 2145 Sheridan Road, Evanston, IL 60208, United States milan.mrksich@northwestern.edu Phone: 847-467-0472 Fax: 847-467-3057 .

that MT are compression resistant and have a role in opposing the pull of the contractile MF network [4]. However, the interplay of IF with MF and MT remains largely unexplored.

IF are composed of one or more members of a large family of proteins subdivided into 5 types: types I/II (keratins), type III (eg, vimentin), type IV (eg, neurofilaments) and type V (nuclear lamins). Vimentin IF (VIF), like many other cytoskeletal IF, forms a complex network that circumscribes the nucleus and radiates toward the cell periphery. There is evidence that VIF are involved in regulating cell motility and polarity [6-10]. For instance, VIF are a key component of cell migration in wound healing as demonstrated by the fact that vimentin-knockout mice are defective in wound healing [8]. Furthermore, the motility of mouse embryonic fibroblasts (MEFs) derived from these mice is impaired, and can be restored by the reintroduction of vimentin [10, 11]. Interestingly, VIF organization is altered upon lamellipodia formation in motile cells where VIF extend throughout the rear and perinuclear region of migrating fibroblasts, but only non-filamentous vimentin particles and short vimentin squiggles are present in the lamellipodial region [7]. Additionally, vimentin-deficient MEFs are impaired mechanically and have reduced contractile capacity [12]. In spite of the evidence supporting the role of VIF in cell motility, the ways in which they cooperate with MF and MT during cell migration is not clear.

To characterize the relationships among the three cytoskeletal elements we used patterned self-assembled monolayers (SAMs) of alkanethiolates on gold to control the shapes and sizes of single cells in culture [13]. These patterned substrates are now well developed for applications in cell biology and have been used to demonstrate the influence of cell spreading on apoptosis [14], the use of local and global geometric cues to direct cytoskeletal distribution and cell polarity [15], the induction of directional motility and polarity across a population of individual cells [16, 17] and the induction of osteogenesis of human mesenchymal stem cells [18]. The use of these patterned substrates permitted quantitative studies of the relationship of VIF, MT, and MF in adherent cells.

Materials and Methods

Micropatterning

A silicon wafer was cleaned and spin coated with SU-8 photoresist (MicroChem), which was patterned using a standard positive photolithography protocol as described [15]. Stamps were prepared by casting polydimethylsiloxane (PDMS) (Dow Corning, Midland, IL) against the photoresist master and curing at 70°C for 8h. The PDMS stamps were inked with octadecanethiol (5 mM in ethanol: Sigma-Aldrich, St Louis, MO), dried under a stream of nitrogen and brought in contact with a gold-coated glass coverslip (prepared by electron beam evaporation of a 50 Å titanium adhesion layer followed by a 500 Å gold layer). After 30 seconds, the stamp was removed from the coverslip which was then incubated in a tri(ethylene glycol)-terminated alkanethiol (5 mM in ethanol: Sigma-Aldrich, St Louis, MO) for 8 h. The coverslips were then washed with ethanol, dried with nitrogen, incubated with 25 g/ml solution of human fibronectin (Invitrogen Carlsbad, CA) in phosphate buffered saline for 2 h and washed with PBS. Cells (~ 10,000 cells/cm^2) were seeded in cell culture medium on the patterned surface.

Cell Culture

The 129/SvJ background, SV40 immortalized wild-type (WT) and vimentin null (vim-/-) MEFs [19] were a generous gift of Dr. J. Eriksson and Dr. E. Torvaldson (Åbo Akademi University and Turku Center for Biotechnology, Turku, Finland). The mouse fibroblasts (NIH/3T3) (ATCC, Manassas, VA), WT and vim-/- MEFs were maintained in high-glucose DMEM supplemented with 10% FBS (Gibco, Gaithersburg, MD) and 1% penicillin/

streptomycin (Gibco). 293FT cells (Invitrogen, Carlsbad, CA) were maintained in high-glucose DMEM supplemented with 10% calf serum (Thermoscientific, Waltham, MA) and 1 % penicillin/ streptomycin. All cells were maintained at 37°C in a humidified CO_2 incubator.

Immunofluorescence

Cells were seeded on the patterned monolayers (~ 10,000 cells/cm^2) for 4-6 h, rinsed with phosphate buffered saline (PBS) and fixed in methanol (−20°C for 5 min) for VIF and MT double labeling or fixed in 3.7% formaldehyde (room temperature for 5 min) for MF labeling. Cells were then processed for immunofluorescence as previously described [20, 21]. The following antibodies were used for immunofluorescence: rabbit anti-vimentin [22], mouse monoclonal anti-γ tubulin (Sigma-Aldrich, Saint Louis MO), rat polyclonal anti-yeast α tubulin (Serotec, Raleigh, NC), mouse anti-vinculin (Sigma-Aldrich) and mouse anti-FLAG (Sigma-Aldrich). MF were labeled with Alexa488 phalloidin (Invitrogen). Secondary antibodies included Alexa488- and Alexa568- conjugated goat anti-rabbit, anti-mouse, and anti-rat. Nuclei were stained with Hoechst 33258 (Invitrogen).

Imaging

Fluorescence images of fixed/stained cells were taken using a Zeiss LSM 510 confocal microscope equipped with a Plan-Apochromat 63x/1.4 oil objective (Carl Zeiss, Jena, Germany). Each image consisted of 10-15 sections of 0.4 - 0.5 m consecutive intervals at 512 × 512 pixel resolution. Maximum intensity projections of the images were exported into ImageJ (NIH, Bethesda, MD) for analysis. To generate heat maps images were aligned, stacked, averaged and pseudo-colored to represent regions of high and low intensity. Cell polarity was determined by first using ImageJ to calculate the centroids of the nuclei and the centrosome and then, using Microsoft Excel, the center of the nucleus was set to zero and the centrosome center was determined relative to the center of the nucleus. The resulting nucleus center – centrosome center vector graph was created and the angle of the nucleus – centrosome vector relative to the horizontal cell axis was calculated. The number of samples in a given 30° increment was determined and the square root of this number was plotted using a polar coordinate plot provided via the ggplot2 package for the open source programming language R.

Plasmids

FLAG-tagged WT **(**pLEX-FLAG-VIM) and mutant (pLEX-FLAG-VIM-Y117L) vimentin were cloned by either PCR amplification of full-length human WT vimentin from pcDNA3-VIM-myc or amplification of full-length human vimentin Y117L from pmCherry-VIM-Y117L (a generous gift from H. Herrmann [23]) and fusing a FLAG tag at the N-terminus. The resulting products were ligated into the BamH1 and Not1 sites of the pLEX vector using an InFusion Kit (Clontech, Mountain View, CA).

Lentivirus Transfection

293FT cells (6×10^5) were seeded into 60 mm dishes and transfected with 3.75 μg psPAX2, 1.25 μg VSV-G and 5 μg of either a control empty vector (pLEX), FLAG-vimentin WT (pLEX-FLAG-VIM) or FLAG-vimentin Y117L (pLEX-FLAG-VIM-Y117L) using Xfect according to the manufacturer's protocol (Clontech). Vim-/- MEFs (6.6×10^4) were seeded into 60 mm dishes and infected with a lentivirus/polybrene (8 μg/mL; Sigma-Aldrich) mixture. After 4-5 h the mixture was exchanged for normal growth medium. After 5 days, the expression was verified by immunofluorescence and immunoblotting and the cells were then used for vimentin rescue experiments.

Gel electrophoresis and immunoblotting

WT and Vim-/- MEFs plated on 60 mm dishes were washed in PBS, solubilized in lysis buffer (1%, SDS, 45 mM Tris pH 6.8, protease inhibitor cocktail (Roche)) and processed for immunoblotting as previously described [7]. Primary antibodies included chicken anti-vimentin (1:5,000, Covance), mouse anti-tubulin (1:5,000, Sigma-Aldrich), mouse anti-actin (1:10,000, Millipore) and mouse anti-FLAG (1:5,000, Sigma-Aldrich). Horseradish peroxidase-conjugated secondary antibodies (KPL, Gaithersburg, MD: goat anti-mouse; Aves Labs, Tigard, Oregon: goat anti-chicken) were used at 1:5,000 and detected with the SuperSignal West Pico Chemiluminescent Substrate kit (Thermo Scientific). Images were collected using the Kodak Image Station 440CF.

Results

Micropatterned Mouse Fibroblasts

We used the microcontact printing method to pattern self-assembled monolayers for the culture of NIH/3T3 cells [13]. This method uses polydimethylsiloxane (PDMS) stamps to transfer octadecanethiol to coverslips coated with an optically transparent layer of gold to give self-assembled monolayers that support the attachment and spreading of individual cells. The remaining regions were modified with a tri(ethylene glycol)-terminated monolayer that prevents the adsorption of protein. The patterned substrate was then treated with a solution of fibronectin to allow adsorption of this matrix protein onto the patterned regions. Cells seeded on these micropatterns attached to the matrix-coated regions and spread to assume the shape of the underlying island.

We first patterned NIH/3T3 cells on substrates having shapes with areas ranging from 600 to 1000 m^2 and found that the 700 m^2 patterns were optimal in that approximately 80% of the islands were occupied by a single cell. We next prepared substrates having a variety of shapes, each with an area of 700 m^2, and we used the substrates to characterize cytoskeletal organization. Cells were allowed to spread on the micropatterns under standard growth conditions for 4-6 h, after which they were fixed either with formaldehyde to preserve MF or methanol to preserve VIF and MT and further processed for immunofluorescence. We collected confocal images of each cytoskeletal element (MF, VIF and MF) for a population of cells (Fig 1, 2). To quantitatively assess the distribution of these cytoskeletal elements across a large population, we individually averaged VIF, MF and MT stains in approximately 50 cells and generated color-coded heat maps—where blue hues represent low frequency of staining and red and pink hues represent high frequency of staining—for each cytoskeletal element and for each shape.

Local versus global control of Cytoskeleton

NIH/3T3 cells adherent to the square shapes had actin stress fibers that assembled along their straight edges (Fig 1A). As observed previously, lamellipodia extended from all sides of the square-shaped pattern with a modest preference for the corners of the shape [15, 24]. Similarly, NIH/3t3 cells plated on circular shapes had stress fibers concentrated at the cell periphery, with lamellipodia extending from all regions of the symmetrical cell perimeter (Fig 1B). The VIF formed a complex network circumscribing the nucleus, and radiating outward in both square and circular cells. We found that for the square-shaped cells, VIF did not extend to the corners (Fig 1A, right top panel). Moreover, the heat maps for both square and circle shaped cells were strikingly similar, both having a prominent perinuclear distribution of VIF (Fig 1A, B). The similarity of VIF on square and circular patterns suggested that this cytoskeletal element does not depend on the presence of corners, and therefore does not respond to local geometrical cues. These observations suggested that the VIF network acts as a global cytoskeletal response system: it does not respond to local

geometric cues, in contrast to MF which is strongly dependent on both local and global geometric cues [15].

We also analyzed the distribution of MT in cells on these two shapes. In both cases MT were concentrated at the microtubule organization center (MTOC) and the overall MT distribution extended relatively evenly throughout the cytoplasm (Fig 1A, B). Previous results have shown that MT networks are non-polarized in cells adherent to square or circle shapes [15]. In agreement with this, our heat maps of MT in square and circle shaped cells showed a homogenous distribution likely due to the random localization of the MTOC (Fig 1A, B).

To further determine the response of the different cytoskeletal systems to cell shape and geometrical influences, we analyzed and compared the distribution of VIF, MT and MF in shapes resembling an arrowhead, teardrop, crescent, dumbbell and rod. Phase contrast and maximum intensity projections of confocal immunofluorescence images were collected for each shape (Fig 2 A-E). The heat maps of VIF and MF showed that the positions of the VIF were inversely related to MF. In the arrowhead, teardrop and crescent shapes, the MF were highly concentrated at the corners and edges of the cell while VIF remained mostly perinuclear,. Further, those filaments that did extend toward the perimeter avoided the sharp corners of the micropatterns, where MF are prominent (Fig 2 A-C). Interestingly, in teardrop shaped cells the VIF were biased toward the blunt edge of the micropattern, likely attributable to the fact that the teardrop shape was the most polarized of the patterns used in our experiments. In elongated shapes like the dumbbell and rod, the MF were concentrated at the cell boundary, while VIF showed a perinuclear distribution with a high concentration along the straight edge of the micropattern (Fig 2E).

MT networks extended throughout the cell regardless of the shape imposed by the different patterns (Fig 2 A-E). The MTOC did not show a significant geometric preference with the exception of the teardrop, where it was primarily located toward the blunt edge of the shape, correlating with a high concentration of MT in this region (Fig 2B). The arrowhead, crescent, dumbbell and rod shapes have less overall polarity and the MT in cells on these shapes were homogenously distributed throughout the cytoplasm. Overall, these observations provide further support that VIF, unlike MF, are global cytoskeletal elements that do not depend on local geometric cues. The VIF and MF appeared inversely related to each other, with regions having concentrated MF corresponding to decreased VIF. Finally, the distribution of MT appears to be mostly dependent on cell polarity.

Micropatterned Vimentin Null Mouse Embryonic Fibroblasts

To determine whether the organization of MF and MT are influenced by VIF, we repeated the analysis described above for wild-type (WT) and vimentin null (vim-/-) MEFs. We also extended our analysis to include the distribution of the focal adhesion protein vinculin. As described above for the NIH/3T3 cells, we first surveyed a range of sizes of the patterned features and found that a size of 1,000 m^2 was optimal for MEFs and therefore used shapes of this size for all experiments. As we found with the NIH/3T3 cells, VIF were concentrated in the nuclear region with a fraction emanating toward the surface in WT MEFs in both teardrop and dumbbell shaped micropatterns (Fig S1 A, B).

We characterized the distribution of MF, vinculin, and MT in WT and vim-/- MEFs on the teardrop and dumbbell patterns (Fig 3A, B). As noted above, the teardrop represents a polarized shape whereas the dumbbell is non-polarized. Heat maps revealed that the MF and vinculin were highly concentrated at the sharp corners and the edges of the WT and vim-/- MEFs in both shapes; that is, these structures were not altered by the absence of vimentin (Fig 3A, B). In contrast, heat maps of MT in WT and vim-/- MEFs revealed that the

distribution of MT was dependent on the presence of VIF in both the teardrop and dumbbell configurations. For example, in confocal images MT appeared somewhat disorganized and reduced in density at the blunt edge of the teardrop and the dumbbell micropattern in vim-/- MEFs (Fig 3A, B). In contrast, both in the teardrop and dumbbell shaped WT MEFs, MT networks were more evenly distributed throughout the cells (Fig 3A, B). Heat maps generated from MT distributions in teardrop and dumbbell shaped cells showed that MT networks were not as closely associated with the blunt edge in the vim-/- cells, while MT networks extended to these blunt edges in WT MEFs. Overall, the heat maps revealed that in both polarized (teardrop) and non-polarized (dumbbell) shapes the absence of VIF caused a loss of the MT density at the blunt edges of the micropattern.

VIF in Cell Polarity and MT Organization

Since the absence of VIF had a strong effect on MT localization and organization, we asked whether the location of the microtubule-organizing center (MTOC or centrosome) and the polarization of the cell were altered in vim-/- cells. The leading edge position of the MTOC relative to the nucleus is a prominent indicator of the polarity of the cell [25]. Earlier work has shown that in ~82% of teardrop-shaped cells, the MTOC is positioned between the nucleus and the cell periphery in the direction of the blunt edge, making this shape a model of a migrating cell [16]. Based on this finding, we hypothesized that while the MTOC should be located on the blunt end side of the nucleus in the teardrop shaped micropattern, in the dumbbell-shaped cells the MTOC should be positioned between the nucleus and either of the two blunt edges of the micropattern.

In order to test this hypothesis and the possible role of VIF, we stained the centrosome with gamma tubulin antibody and nuclei with Hoechst in teardrop and dumbbell-shaped WT and vim-/- MEFs. We determined the centroid positions of the nucleus and the centrosome from maximum intensity confocal image projections of each cell and plotted the resulting vectors. For cells on the teardrop pattern, ~ 70% of WT MEFs were polarized towards the blunt edge of the micropattern. In contrast, the centrosomes in vim-/- MEFs were randomly positioned with ~40% toward the blunt edge (Fig 4A). We also determined the angle between the nucleus – centrosome vector and the horizontal axis of the cell. This nucleus – centrosome angle, which was plotted in polar coordinates, showed that the majority of the WT MEFs in a teardrop shape were polarized to 0° (±15 degrees) in the direction of the blunt edge, while vim -/- MEFs had centrosomes which were present at a wide array of angles (Fig 4B). The non-polarized dumbbell shape had two blunt edges and the resulting vector plots and the polar coordinate plots in both WT and vim-/- MEFs showed random positioning of the centrosome. Our analysis agrees with previous findings demonstrating vim-/- MEFs have impaired motility compared to WT MEFs [25].

As there were apparent defects in the nucleus – centrosome axis in the absence of VIF, we next determined the position of the centrosome with respect to the center of the cell. We found that the position of the nucleus did not change in WT and vim-/- MEFs in teardrop and dumbbell shaped cells (Fig S2A, C, E). However, the centrosome position had a higher degree of variability in vim-/- MEFs in both shapes (Fig SB, D) and there was a statistically significant difference in centrosome deviation from the center of the teardrop shaped cells (vim-/- MEFs 3.97 m ± 2.68 as compared to WT MEF 2.82 m ± 1.62; $p<0.01$) (Fig S2E). This analysis further supports the conclusion that the absence of VIF perturbs the overall polarity of cells as determined by centrosome positioning.

We stably expressed FLAG-tagged vimentin using a lentivirus vector in the vim-/- MEFs. To determine whether it was filamentous vimentin as opposed to vimentin protein that stabilized the MT network, we also expressed the unit-length-filament mutant VIM-Y117L. This mutant arrests assembly of filaments at the ULF stage, preventing the formation of VIF

[23]. For cells adherent to the polarized teardrop shape we confirmed that FLAG-VIM WT formed IF while FLAG-VIM-Y117L only formed particles; both were expressed at similar levels in vim-/- MEFs (Fig S3A, C).

The expression of WT vimentin, but not the ULF mutant restored MT organization (Fig 5A) and cellular polarity (Fig 5B, C). Heat maps of MT in vim-/- MEFs in teardrop shapes showed a sparse localization toward the blunt edge when transfected with either the control vector or the FLAG-VIM Y117L mutant, while FLAG-VIM WT restored MT density at the blunt edge (Figure 5A; see supplement S4 for individual examples). The centrosome location was also rescued by reintroduction of WT-vim, but not the ULF mutant in the teardrop shaped cells. Expression of FLAG-VIM WT, but not the vector or FLAG-VIM Y117L (Fig 5B) was also able to restore the nucleus – centrosome relationship (Fig 4A). Furthermore, the angle of the nucleus – centrosome vector in the ULF mutant transfected cells was distributed across an array of angles, while in the VIM-WT expressing cells the nucleus – centrosome angles were highly weighted towards the blunt edge (Fig 5C) as in WT MEFs (Fig 4B).

Discussion

This work reports the results of quantitative studies of the interdependence of cytoskeletal networks in patterned cells. We specifically focused on VIF and its role in regulating cell polarity and influencing the structures of other cytoskeletal networks. Studies of the cytoskeleton are difficult because these structures are heterogeneous and depend on cell shape. Indeed, there is contradictory evidence in the literature on the importance of IF in maintaining cell mechanical properties and its role in directing cell polarity as related to the motile properties of cells. One study reported no changes in motility or mechanical properties [26], while other studies showed reduced mechanical stability and both random and directed motility in vim-/- MEFs [10-12]. Furthermore, reactive astrocytes devoid of GFAP IF and VIF exhibit clear morphological changes and profound defects in cell motility [6]. We previously showed that the silencing of vimentin and the loss of IF results in fibroblasts with a more rounded epithelial-like morphology. These cells form lamellipodial structures across the entire cell periphery with a loss of cell polarity and a significant reduction in cell motility [7, 11]. Given these disparate results, it is obvious that basic studies of the interactions among the three major cytoskeletal systems are required in order to gain a more complete understanding of the complexities involved in cell shape, motility and cell polarity. The present paper addresses the broad question of whether the three-cytoskeletal elements are interdependent on each other with a specific interest in the role of VIF.

We first compared the cytoskeletal structures for VIF, MF and MT in 3T3 cells that were patterned in a variety of shapes and found that unlike MF, the VIF do not respond to subtle changes in shape. For example, the MF heat maps make it easy to discern square from circle shapes as MF localize at the sharp corners and the straight edges of the square, while MF are enriched at the circumference of the circular cell. In contrast, VIF in these two shapes are mainly perinuclear with a fraction emanating to the cell surface; making it difficult to discern square from circle based on VIF patterns alone. The MT network extends evenly throughout the cells in these two shapes. We also characterized the cytoskeletons in cells patterned in a variety of asymmetric shapes. We found that MF respond to both local and global geometric clues, with greater localization at the corners of the shape and along the long edges of the shapes, while VIF tend to remain largely perinuclear and therefore show little dependence on geometric cues. The MT networks on these asymmetric patterns are evenly distributed throughout the cells with the exception of the teardrop shaped pattern where MT are primarily concentrated toward the blunt edge of the shape. Within

asymmetric shapes VIF tend to avoid areas of large MF concentration, such as the pointed edge of the teardrop or crescent. These observations agree with our previous report that in serum-starved cells, VIF extend to the periphery of fibroblasts and lamellipodia formation is inhibited. After serum addition, disassembly and withdrawal of mature VIF occurs in the cell periphery and subsequently actin-rich lamellipodia form [7]. The heat maps support these observations that VIF avoid the branched actin networks present in regions where lamellipodia form, but do not avoid the MF stress fibers such as those present along the long axis of the rod shape.

One of the asymmetric shapes, the teardrop, showed that the localization of VIF was biased toward the blunt edge. A previous study used this shape as a model of a migrating cell, and showed that when released from the shape, 82 % of cells migrated in the direction of the curved edge [16]. Our studies on this polarized shape revealed that in addition to VIF, MT are also biased toward the migrating edge, being concentrated at the MTOC. The MTOC has been found in numerous cell types to localize in front of the nucleus in the direction of migration [16] and to contain a large concentration of VIF and MT [27]. The mechanisms that account for this co-localization of the VIF with the MTOC are not clear; although it is possible that VIF could contribute to the stabilization of the centrosome connection to and association with the nucleus.

Our investigation of the distribution of cytoskeletal elements on a non-polarized (dumbbell) and a polarized (teardrop) shape in both WT and vim -/- cells demonstrates that the localization of MF and focal adhesions remain unaltered in the absence of VIF. In contrast, MT in vim-/- MEFs cultured on these shapes are clearly altered as evidenced by a significant reduction in their concentration in the blunt or migratory edge of both of these micropatterns. This finding is consistent with the known interactions between VIF and MT. For example, VIF and MT are closely associated when observed by both light and electron microscopy [28] and the disruption of MT by nocodazole leads to a retraction of the majority of VIF towards the nucleus [28]. We note that a previous study addressing the regulation of the MT network in vimentin null cells has concluded that the MT network remains unaffected [26]. However, that study was carried out without the advantage of micropatterned substrates, which can reveal cytoskeletal relationships that are difficult to identify in typical cell culture conditions.

Our results also show that VIF play a role in establishing cell polarity with respect to the nucleus – centrosome axis. While centrosome dispersion is evident in both the teardrop and dumbbell shaped cells, the directional polarity is only perturbed in the teardrop shaped vim -/-MEFs (Fig 4). This defect in vim-/- cell polarity could be related to the loss of the VIF/nesprin-3 complex. Nesprin-3 has been proposed to maintain VIF in their proper perinuclear localization and to anchor the centrosome in close proximity to the nucleus [29]. It is possible, therefore, that the VIF/Nesprin-3 complex in WT cells is important for maintaining proper centrosome positioning and a proper response to cell polarity cues.

Conclusions

We have used micropatterned substrates to create populations of cells having a uniform shape and have analyzed these populations to assess the interactions among VIF, MF and MT in fibroblasts. The use of patterned substrates reduces the significant heterogeneity in cell shape inherent in actively growing cell cultures. The use of patterns also permits quantitative studies of the relationship between cell shape and the different cytoskeletal systems. The results reveal a dependence of MT-based cell polarity and MT organization on VIF and further reveal that VIF, unlike MF, are a global structure that does not respond to subtle changes in cell shape. The results of this study demonstrate the importance of

imposing defined cell shapes to determine the relationships among the three major cytoskeletal networks in vertebrate cells.

Supplementary Material

Refer to Web version on PubMed Central for supplementary material.

Acknowledgments

SHS is supported by NIH and MMC is supported by NIH/NHLBI training grant T32HL076139 and R. D. Goldman is supported by NIH 5P01GM096971-02. This work was funded in part by the Chicago Biomedical Consortium with support from the Searle Funds at The Chicago Community Trust. We acknowledge Dr. B. Grin for preparing the lentivirus vectors, Dr. V. Gelfand for thoughtful advice, Dr. H. Herrmann for the ULF mutant, Dr. J. Eriksson and his graduate student E. Torvaldson for the WT and vim-/- cells and J. Harwig for help writing the code to plot the polar coordinates of the centrosome location.

References

[1]. Yang Y, Bauer C, Strasser G, Wollman R, Julien J-P, Fuchs E. Integrators of the cytoskeleton that stabilize microtubules. Cell. 1999; 98:229–38. [PubMed: 10428034]

[2]. Karakesisoglou I, Yang Y, Fuchs E. An epidermal plakin that integrates actin and microtubule networks at cellular junctions. J Cell Biol. 2000; 149:195–208. [PubMed: 10747097]

[3]. Klymkowsky WM. Weaving a tangled web: the interconnected cytoskeleton. Nat Cell Biol. 1999; 1:E121–E3. [PubMed: 10559951]

[4]. Ingberg ED. Cellular tensegrity:defining new rules of biological design that govern the cytoskeleton. J Cell Sci. 1993; 104:613–27. [PubMed: 8314865]

[5]. Waterman-Storer CM, Salmon ED. Positive feedback interactions between microtubule and actin dynamics during cell motility. Curr Opin Cell Biol. 1999; 11:61–7. [PubMed: 10047528]

[6]. Lepekhin EA, Eliasson C, Berthold C-H, Berezin V, Bock E, Pekny M. Intermediate filaments regulate astrocyte motility. J Neurochem. 2001; 79:617–25. [PubMed: 11701765]

[7]. Helfand BT, Mendez MG, Murthy SNP, Shumaker DK, Grin B, Mahammad S, et al. Vimentin organization modulates the formation of lamellipodia. Mol Biol Cell. 2011; 22:1274–89. [PubMed: 21346197]

[8]. Gilles C, Polette M, Zahm JM, Tournier JM, Volders L, Foidart JM, et al. Vimentin contributes to human mammary epithelial cell migration. J Cell Sci. 1999; 112:4615–25. [PubMed: 10574710]

[9]. Phua DCY, Humbert PO, Hunziker W. Vimentin regulates scribble activity by protecting it from proteasomal degradation. Mol Biol Cell. 2009; 20:2841–55. [PubMed: 19386766]

[10]. Eckes B, Colucci-Guyon E, Smola H, Nodder S, Babinet C, Krieg T, et al. Impaired wound healing in embryonic and adult mice lacking vimentin. J Cell Sci. 2000; 113:2455–62. [PubMed: 10852824]

[11]. Mendez MG, Kojima S-I, Goldman RD. Vimentin induces changes in cell shape, motility, and adhesion during the epithelial to mesenchymal transition. FASEB J. 2010; 24:1838–51. [PubMed: 20097873]

[12]. Eckes B, Dogic D, Colucci-Guyon E, Wang N, Maniotis A, Ingber D, et al. Impaired mechanical stability, migration and contractile capacity in vimentin-deficient fibroblasts. J Cell Sci. 1998; 111:1897–907. [PubMed: 9625752]

[13]. Mrksich M, Dike LE, Tien J, Ingber DE, Whitesides GM. Using microcontact printing to pattern the attachment of mammalian cells to self-assembled monolayers of alkanethiolates on transparent films of gold and silver. Exp Cell Res. 1997; 235:305–13. [PubMed: 9299154]

[14]. Chen CS, Mrksich M, Huang S, Whitesides GM, Ingber DE. Geometric control of cell life and death. Science. 1997; 276:1425–8. [PubMed: 9162012]

[15]. James J, Goluch ED, Hu H, Liu C, Mrksich M. Subcellular curvature at the perimeter of micropatterned cells influences lamellipodial distribution and cell polarity. Cell Motil Cytoskel. 2008; 65:841–52.

[16]. Jiang X, Bruzewicz DA, Wong AP, Piel M, Whitesides GM. Directing cell migration with asymmetric micropatterns. Proc Natl Acad Sci USA. 2005; 102:975–8. [PubMed: 15653772]

[17]. Théry M, Racine V, Piel M, Pépin A, Dimitrov A, Chen Y, et al. Anisotropy of cell adhesive microenvironment governs cell internal organization and orientation of polarity. Proc Natl Acad Sci USA. 2006; 103:19771–6. [PubMed: 17179050]

[18]. Kilian KA, Bugarija B, Lahn BT, Mrksich M. Geometric cues for directing the differentiation of mesenchymal stem cells. Proc Natl Acad Sci USA. 2010; 107:4872–7. [PubMed: 20194780]

[19]. Colucci-Guyon E, Portier M-M, Dunia I, Paulin D, Pournin S, Babinet C. Mice lacking vimentin develop and reproduce without an obvious phenotype. Cell. 1994; 79:679–94. [PubMed: 7954832]

[20]. Jaeger RG, Jaeger MMM, Araujo VC, Kachar B. Analysis of the interdependent localization of vimentin and microtubules in neoplastic myoepithelial cells. Cell Motil Cytoskel. 1995:289–98.

[21]. Grin B, Mahammad S, Wedig T, Cleland MM, Tsai L, Herrmann H, et al. Withaferin A alters intermediate filament organization, cell shape and behavior. PLoS ONE. 2012; 7:e39065. [PubMed: 22720028]

[22]. Helfand BT, Mikami A, Vallee RB, Goldman RD. A requirement for cytoplasmic dynein and dynactin in intermediate filament network assembly and organization. J Cell Biol. 2002; 157:795–806. [PubMed: 12034772]

[23]. Meier M, Padilla GP, Herrmann H, Wedig T, Hergt M, Patel TR, et al. Vimentin coil 1A— A molecular switch involved in the initiation of filament elongation. J Mol Biol. 2009; 390:245–61. [PubMed: 19422834]

[24]. Parker KK, Brock AL, Brangwynne C, Mannix RJ, Wang N, Ostuni E, et al. Directional control of lamellipodia extension by constraining cell shape and orienting cell tractional forces. FASEB J. 2002; 16:1195–204. [PubMed: 12153987]

[25]. Hale CM, Chen W-C, Khatau SB, Daniels BR, Lee JSH, Wirtz D. SMRT analysis of MTOC and nuclear positioning reveals the role of EB1 and LIC1 in single-cell polarization. J Cell Sci. 2011; 124:4267–85. [PubMed: 22193958]

[26]. Holwell TA, Schweitzer SC, Evans RM. Tetracycline regulated expression of vimentin in fibroblasts derived from vimentin null mice. J Cell Sci. 1997; 110:1947–56. [PubMed: 9296393]

[27]. Trevor KT, McGuire JG, Leonova EV. Association of vimentin intermediate filaments with the centrosome. J Cell Sci. 1995; 108:343–56. [PubMed: 7738109]

[28]. Goldman RD. The role of three cytoplasmic fibers in BHK-21 cell motility: I. microtubules and the effects of colchicine. J Cell Biol. 1971; 51:752–62. [PubMed: 4942774]

[29]. Morgan JT, Pfeiffer ER, Thirkill TL, Kumar P, Peng G, Fridolfsson HN, et al. Nesprin-3 regulates endothelial cell morphology, perinuclear cytoskeletal architecture, and flow-induced polarization. Mol Biol Cell. 2011; 22:4324–34. [PubMed: 21937718]

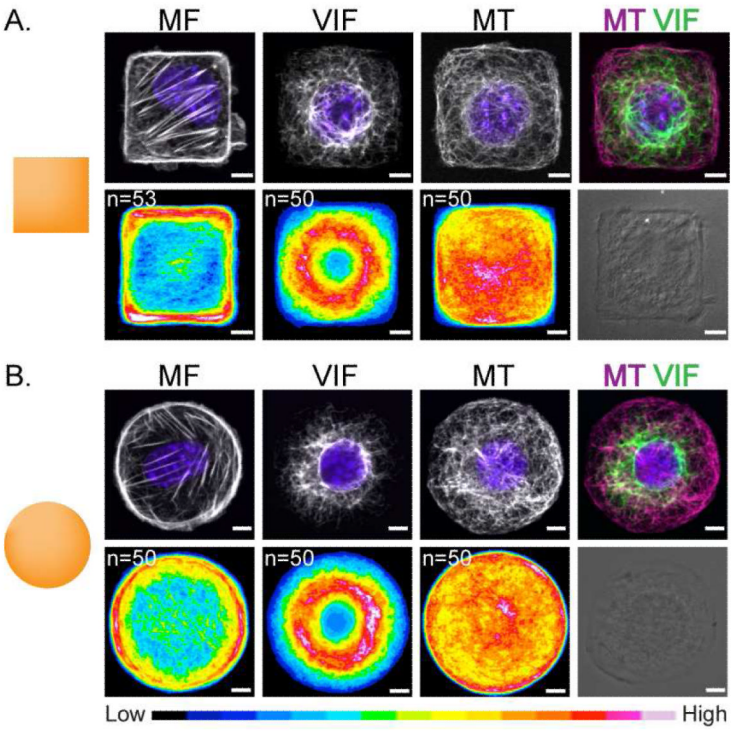

Figure 1. VIF is a global cytoskeletal element

Immunofluorescence /phase images of NIH/3T3 cells patterned on 700 μm^2 micropatterns. MF, VIF, MT and nuclei (blue) were stained as described in Materials and Methods. Cell population heat maps of MF, VIF and MT were generated using Image J for square (A) and circle (B) shaped cells. n=number of cells used to generate the heat map. Scale bar is 5 μm.

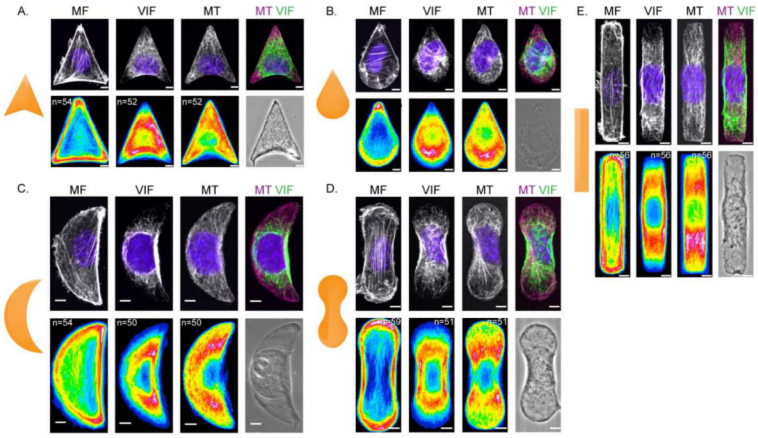

Figure 2. VIF distribution on complex shapes

Immunofluorescence /phase images of NIH/3T3 cells patterned on 700 μm^2 micropatterns. MF, VIF, MT and nuclei (blue) were stained as described in Materials and Methods. Cell population heat maps of MF, VIF and MT were generated using Image J for arrowhead (A), teardrop (B), crescent (C), dumbbell (D) and rod (E) shaped cells. n is the number of cells used to generate the heat map. Scale bar = 5 μm.

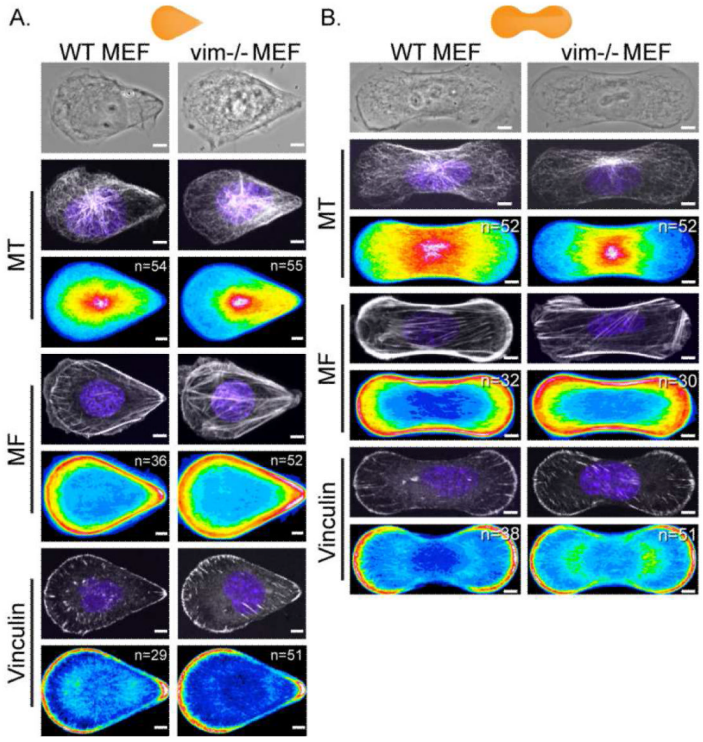

Figure 3. Absence of VIF results in the disorganization of the MT network

Immunofluorescence /phase images of WT and vim-/- MEFs cells patterned on 1000 μm^2 micropatterns. MT, MF, vinculin (to mark focal adhesion) and nuclei (blue) were stained as described in Materials and Methods. Cell population heat maps of MT, MF and vinculin were generated using Image J for teardrop (A) and dumbbell (B) shaped cells. n is the number of cells used to generate the heat map. Scale bar = 5 μm.

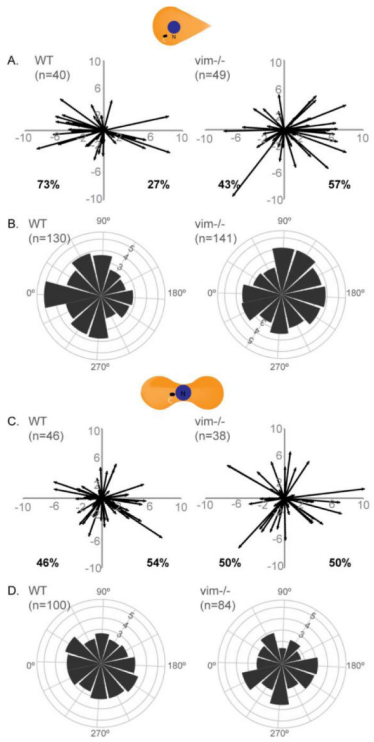

Figure 4. Absence of VIF affects cell polarity

WT and vim-/- MEFs were seeded on 1000 μm^2 micropatterns of teardrop (A, B) or dumbbell (C, D) shapes. The cells were stained with gamma-tubulin to mark the centrosome and Hoechst to locate the nucleus. The (x,y) coordinates for the center of the nucleus and center of the centrosome were calculated using ImageJ. The nucleus center – centrosome center vectors was then plotted for the teardrop (A) and dumbbell (C) shapes (See Materials and Methods). For each cell type/shape (B & D), the vectors were converted into angles and the number of samples in a given 30-degree increment was determined and the square root of this number was plotted on a polar coordinate plot (See Materials and Methods). n=number of cells used to generate the plots.

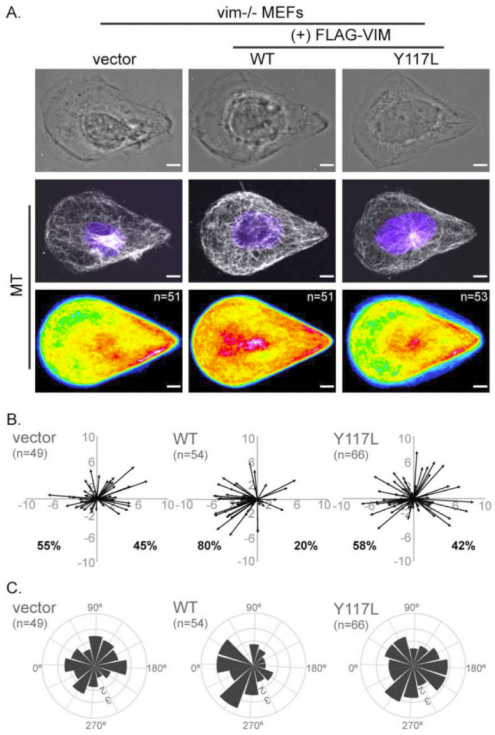

Figure 5. VIF are essential for MT organization and cell polarity

VIF (+FLAG-Vimentin WT), the ULF mutant (+FLAG-Vimentin Y117L) or a vector control was expressed in vim-/- MEFs and the cells then were seeded on teardrop shape micropatterns. Immunofluorescence/phase images of MT and nuclei (blue) were collected and cell population heat maps of MT were generated in Image J (A). Cell polarity was analyzed by plotting vectors for nucleus center and centrosome center calculated in Image J (B) (see Materials and Methods; also Figure 4). The vectors were converted into angles and polar coordinate plots were generated for each system (C) (see Materials and Methods; also Figure 4). n = number of cells used to generate the data. Scale bar = 5 μm.